CellPress
OPEN ACCESS

Article

δ-Protocadherins regulate neural progenitor cell division by antagonizing Ryk and Wnt/β-catenin signaling

Sayantanee Biswas, Michelle R. Emond, Kurtis P. Chenoweth, James D. Jontes

jontes.1@osu.edu

Highlights

Loss of individual δ-pcdhs leads to elevated proliferation in the zebrafish hindbrain

Zebrafish mutants lacking δ-pcdhs show elevated Wnt/β-catenin signaling

Inhibiting Wnt/β-catenin signaling blocks elevated proliferation in δ-pcdh mutants

The Wnt receptor Ryk is required for the elevated proliferation in δ-pcdh mutants

Article

δ-Protocadherins regulate neural progenitor cell division by antagonizing Ryk and Wnt/β-catenin signaling

Sayantanee Biswas,[1,2] Michelle R. Emond,[1,2] Kurtis P. Chenoweth,[1] and James D. Jontes[1,3,*]

SUMMARY

The division of neural progenitor cells provides the cellular substrate from which the nervous system is sculpted during development. The δ-protocadherin family of homophilic cell adhesion molecules is essential for the development of the vertebrate nervous system and is implicated in an array of neurodevelopmental disorders. We show that lesions in any of six, individual δ-protocadherins increases cell divisions of neural progenitors in the hindbrain. This increase is due to mis-regulation of Wnt/β-catenin signaling, as this pathway is upregulated in δ-protocadherin mutants and inhibition of this pathway blocks the increase in cell division. Furthermore, the δ-protocadherins can be present in complex with the Wnt receptor Ryk, and Ryk is required for the increased proliferation in protocadherin mutants. Thus, δ-protocadherins are novel regulators of Wnt/β-catenin signaling that may control the development of neural circuits by defining a molecular code for the identity of neural progenitor cells and differentially regulating their proliferation.

INTRODUCTION

The regulated production of new cells through cell division and their differentiation into new cell types is one of the primary driving forces in the development of multicellular organisms. The correct number of new cells and cell types must be temporally and spatially regulated during development. The canonical Wnt/β-catenin pathway plays prominent roles in regulating cell proliferation during development, and mutations in components of this pathway contribute to cancers and neurodevelopmental disorders (Cadigan and Liu, 2006; Clevers, 2006; De Ferrari and Moon, 2006; Kwan et al., 2016; MacDonald et al., 2009; Nusse and Clevers, 2017). However, the mechanisms providing spatiotemporal context to the regulation of proliferation and Wnt/β-catenin signaling are less well understood.

The δ-protocadherins (δ-pcdhs) are homophilic cell adhesion molecules within the cadherin superfamily (Bisogni et al., 2018; Cooper et al., 2016; Harrison et al., 2020) that are subdivided into δ1 and δ2 subfamilies on the basis of the number of extracellular cadherin repeats (seven for δ1-pcdhs and six for δ2-pcdhs) and have conserved sequence motifs in their intracellular domains (Hulpiau and van Roy, 2011; Vanhalst et al., 2005). In the zebrafish, there are six δ1-pcdhs (*pcdh1a*, *pcdh1b*, *pcdh7a*, *pcdh7b*, *pcdh9*, and *pcdh11*) and six δ2-pcdhs (*pcdh10a*, *pcdh10b*, *pcdh17*, *pcdh18a*, *pcdh18b*, and *pcdh19*), as well as the δ2-like paraxial protocadherin. The δ-pcdhs are essential for neural development, as they have been implicated in a wide range of neurodevelopmental disorders (Hirano and Takeichi, 2012; Redies et al., 2012), including autism spectrum disorders (Bruining et al., 2015; Morrow et al., 2008; Piton et al., 2011) and epilepsy (Depienne et al., 2009; Dibbens et al., 2008; Lal et al., 2015; Perez-Palma et al., 2017). Mutations in the δ2-pcdh, *PCDH19*, result in a female-limited form of infant-onset epilepsy (Depienne et al., 2009; Dibbens et al., 2008), making *PCDH19* the second most commonly affected gene in epilepsies (Depienne and LeGuern, 2012). As well as their importance for brain development, the δ-pcdhs are intimately associated with cancer (Berx and van Roy, 2009; van Roy, 2014). Expression of δ-pcdhs is downregulated in multiple cancer cell lines with various examples of silencing by promoter methylation (Tang et al., 2012; Zhang et al., 2017). Moreover, prognosis correlates with levels of δ-pcdh expression (Bing et al., 2018), whereas invasion and metastasis correlate with δ-pcdh loss (Lin et al., 2018). In addition, there is evidence that expression of δ-pcdhs can inhibit tumor growth through regulating Wnt/β-catenin signaling (Xu et al., 2015; Yin et al., 2016; Zong et al., 2017). Finally, the

[1]Department of Neuroscience, Ohio State University Wexner Medical Center, Columbus, OH 43210 USA

[2]These authors contributed equally

[3]Lead contact

*Correspondence: jontes.1@osu.edu

clustered protocadherin γ-C3 isoform can interact with Axin to inhibit canonical Wnt signaling (Mah et al., 2016).

Members of the δ-pcdh family fulfill a variety of roles during development, including the regulation of morphogenetic cell movements (Aamar and Dawid, 2008; Biswas et al., 2010; Chen and Gumbiner, 2006; Emond et al., 2009; Kim et al., 1998; Kraft et al., 2012; Williams et al., 2018), axon outgrowth and guidance (Biswas et al., 2014; Hayashi et al., 2014; Leung et al., 2013; Piper et al., 2008), and dendrite morphogenesis (Wu et al., 2015). Here, we show that, in zebrafish, the δ-pcdh family regulates cell proliferation in the developing neuroepithelium, suggesting that regulation of cell division is a core function for this family of proteins. In addition, we provide evidence that δ-pcdhs influence cell proliferation by regulating Wnt/β-catenin signaling, as the canonical Wnt pathway is elevated in each of the δ-pcdh mutants, and inhibiting this pathway blocks the elevated cell proliferation observed in these mutants. We further show that the Wnt receptor Ryk physically interacts with the δ-pcdhs and is required for the increased proliferation. These results suggest that the δ-pcdhs are novel upstream regulators of canonical Wnt/β-catenin signaling and provide a link between their biological role and their involvement in neurodevelopmental disorders and cancers.

RESULTS

The δ-pcdhs regulate proliferation of neuroepithelial cells

We previously showed that zebrafish *pcdh19* is expressed in neural progenitor cells in the zebrafish optic tectum and that Pcdh19 regulates proliferation. Mutant embryos lacking *pcdh19* exhibited an increased proliferation, as assessed by EdU labeling and phospho-Histone H3 (pH3) immunostaining (Cooper et al., 2015). The increased proliferation was accompanied by an increased number of *pcdh19* + neurons. Similar results have been obtained for mouse *pcdh11x*, which negatively regulates proliferation and neurogenesis in mouse cortex (Zhang et al., 2014). Pcdh19 and Pcdh11x are members of the δ-pcdh family, δ2-and δ1-pcdh subfamilies, respectively (Figure 1A). To determine if other members of the δ-pcdh family play a similar role, we used CRISPR-Cas9 to make targeted lesions in the extracellular domains of *pcdh1a*, *pcdh7a*, *pcdh9*, and *pcdh17* (Figure S1). We used TALENs to generate mutations in *pcdh18b* and previously reported TALEN-mediated lesions in *pcdh19* (Cooper et al., 2015). Thus, we generated mutant lines for three of six δ1-pcdhs and three of six δ2-pcdhs. All of these mutants are homozygous viable and fertile; embryos used in our experiments were obtained from incrosses of homozygous adults. Like *pcdh19*, each of the other δ-pcdhs is expressed in the neuroepithelium at this stage of development, 18 h post fertilization (hpf), and at later stages (e.g., 48 hpf) (Figure S2). To assess the roles of these δ-pcdhs in regulating proliferation, we performed immunostaining for the M phase marker pH3 and counted the total number of pH3+ cells in image stacks of the hindbrains of 18-hpf embryos (Figures 1B–1D). As shown previously in the optic tectum, loss of *pcdh19* resulted in an increase in pH3+ cells in the hindbrain, which was rescued by forced expression of Pcdh19-GFP (Figure 1E) (*wild type*, 157 ± 5, n = 25; *pcdh19-/-*, 216.7±8.9 n=20; *pcdh19-/- +heat shock* 155.5±11.2, n=9). For each δ-pcdh that we tested, we also observed an elevation in mitotic profiles (Figure 1F) (*wild type*, 157±5, n=25; *pcdh1a-/-*, 216.7±8.9 n=20; *pcdh7a-/-*, 192.9±8, n=17; *pcdh9-/-*, 203.6±6.9, n=16; *pcdh17-/-*, 211.1±8.7, n=17; *pcdh18b-/-*, 203.5±6.6, n=20; *pcdh19-/-*, 223.7±5.1, n=37). As phospho-Histone H3 is an M phase marker, it is possible that the elevated labeling observed in our mutants is due to an arrest or lengthening of M phase, rather than an increase in cell division. To address this, we used *in vivo* timelapse imaging to visualize cell divisions in the neuroepithelium of wild-type and *pcdh18b* mutant embryos (Figure 2). A BAC clone harboring the *pcdh18b* gene was previously modified to express Gal4-VP16 (*BAC(pcdh18b:Gal4)*) (Cooper et al., 2015). This BAC clone was used to co-express Histone H2A-GFP and Lifeact-GFP in the hindbrains of 18-hpf embryos (Figure 2A). Timelapse imaging allowed the identification and characterization of dividing cells (Figure 2B). From these movies (Video S1), we measured the length of M phase, defined as the time of initial rounding of the nucleus through the completion of cytokinesis (Figure 2C) (*wild type*, 21.6±0.4 min, n=155; *pcdh18b*$^{-/-}$, 20.7±0.3 min, n=167; p=0.0849). The measured M phase durations are similar to previously reported measurements (Leung et al., 2011) and show that there is not an arrest or delay of M phase in *pcdh18b* mutants (Video S2). These results support the conclusion that the loss of δ-pcdhs leads to an increase in the number of neural progenitor cells entering mitosis.

To determine the impact of δ-pcdh loss on hindbrain organization we visualized the distribution of *pcdh19*+ cells in the hindbrains of BAC transgenic larvae expressing Histone H2A-GFP under the control of *pcdh19* regulatory elements, *TgBAC(pcdh19-0.5hsp70: H2A-GFP)^{os75Tg}*. At 3 dpf, H2A-GFP was expressed in bilateral clusters of cells, as well as lateral columns of motor neurons (Figure 3). When expressed
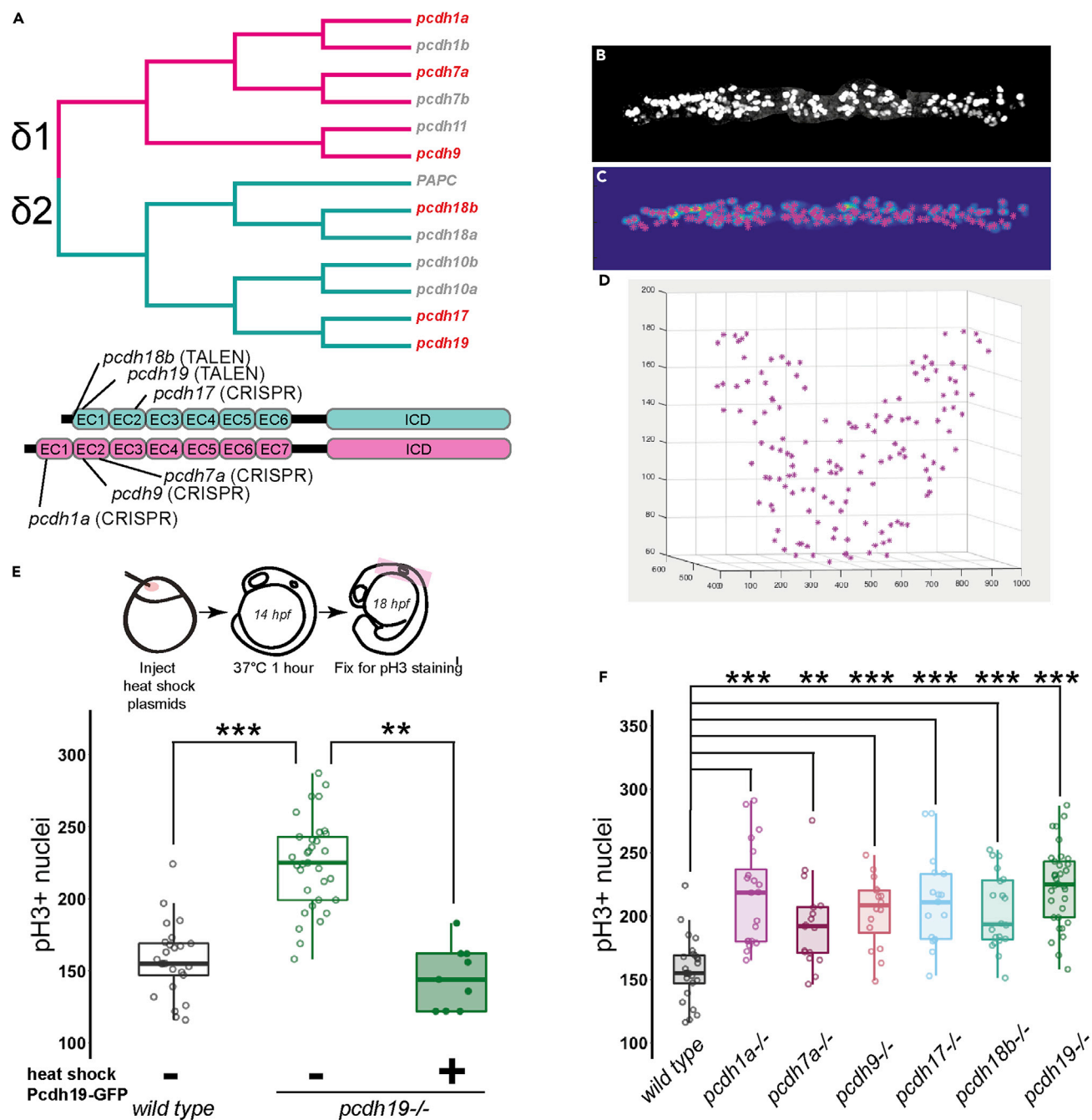
Figure 1. The δ-pcdhs regulate proliferation of neuroepithelial cells

(A) Overview of the δ-pcdhs. The δ-pcdhs are divided into two subfamilies, the δ1-and δ2-pcdhs, which differ by the presence of seven or six extracellular cadherin repeats, respectively. In both cases, the adhesive interface includes the four distal extracellular domains (as shown). Mutations were generated for six δ-pcdhs (shown in red) and the target sites for each are highlighted. All lesions are within the first two extracellular domains. See also Figures S1 and S2.

(B) A maximum intensity projection of a wild-type 18 hpf embryo labeled with an antibody against phospho-HistoneH3. Analysis was restricted to the neural tube by manually masking out nuclei on the skin or yolk.

(C and D) Labeled cells are identified by 3D cross-correlation.

(E) The number of pH3+ nuclei is elevated in pcdh19 mutants relative to wild-type embryos (WT, n = 25; pcdh19-/-, n=35; ***p<0.0001, two-tailed Student's t test) but is rescued by forced expression of Pcdh19 in the pcdh19 mutants (pcdh19-/-, n=35; pcdh19 hs, n=9; **p<0.001, two-tailed Student's t test). Error bars represent the mean +/- standard error (SEM).

(F) Each δ-pcdh mutant shows elevated pH3 labeling, relative to wild-type embryos. (WT, n=25; pcdh1a-/-, n=20, ***p<0.0001; pcdh7a-/-, n=17, **p=0.0097; pcdh9-/-, n=16, ***p=0.0003; pcdh17-/-, n=17, ***p<0.0001; pcdh18b-/-, n=20, ***p<0.0001; pcdh19-/-, n=38, ***p<0.0001, one-way ANOVA with Tukey HSD). Error bars represent the mean +/- standard error (SEM).
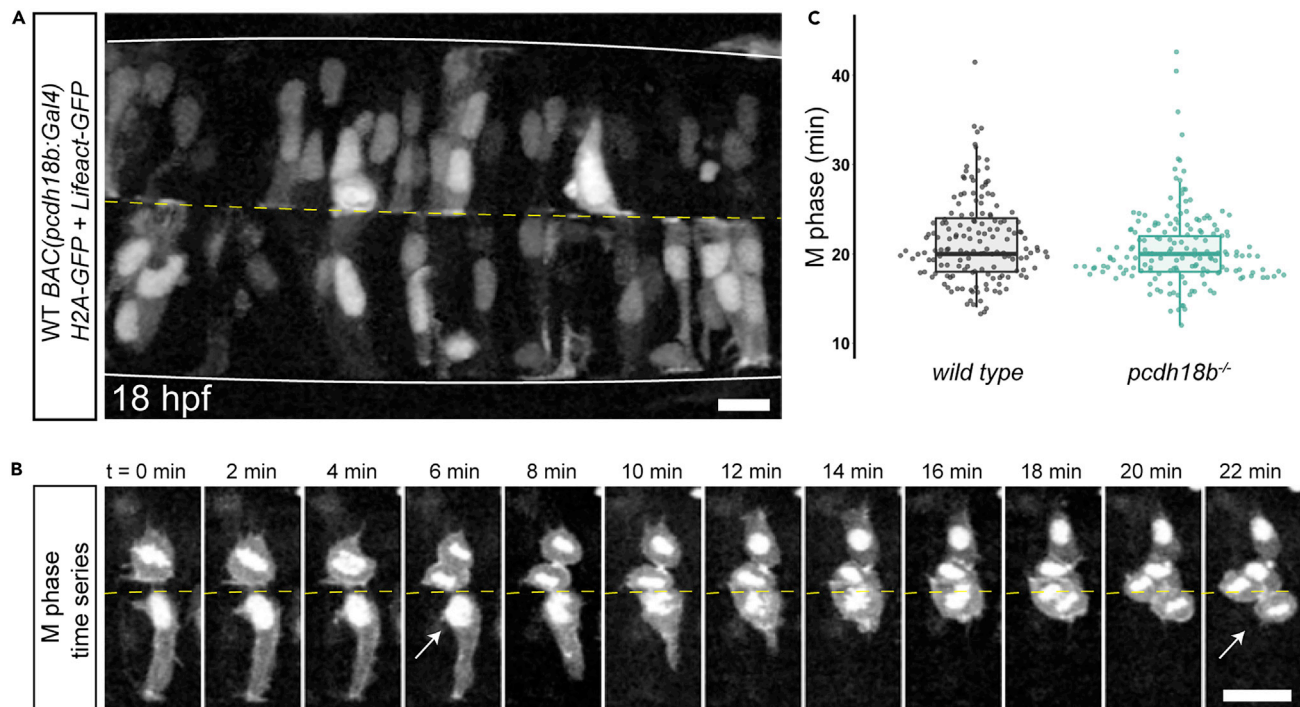
Figure 2. Measurement of M phase by timelapse imaging

(A) An optical section from an image stack from an 18 hpf wild-type embryo that was injected with BAC(pcdh18b:Gal4-VP16) and a UAS plasmid to co-express H2A-GFP to label nuclei and Lifeact-GFP to label F-actin. Scale bar, 10 μm.

(B) A timelapse image sequence showing two cell divisions along the midline. In the bottom half of the image, the nucleus of the neuroepithelial cell rounds up, the cell detaches from the basal side of the of the neuroepithelium and rounds, before the cell proceeds through metaphase, anaphase, then cytokinesis. The duration of M phase was measured as the time encompassing the initial rounding up of the nucleus through cytokinesis (arrows). Scale bar, 10 μm.

(C) M phase was measured in wild-type and pcdh18b-/- embryos, revealing no significant difference in the duration of M phase. (WT, n=155 divisions from three embryos; pcdh18b-/-, n = 167 divisions from three embryos; p = 0.0849, two-tailed Student's t test).

in a *pcdh19-/-* background, we observed an elevated number of H2A-GFP labeled cells in the BAC transgenic line (Figures 3B and 3D) compared with wild type (Figures 3A and 3C). There was an ∼24% increase in the number of fluorescently labeled cells (Figure 3E) in the *pcdh19* mutants (wild type, n = 679.8 ± 49.8 cells, n = 5; *pcdh19-/-*, n = 843.7 ± 29.6, n = 7; p = 0.013). This is similar to what we previously reported for the optic tectum (Cooper et al., 2015). Thus, the observed increase in mitotic profiles found in earlier developmental timepoints leads to an increase in neurogenesis within the population of cells that normally expresses the inactivated δ-pcdh.

The δ-pcdhs coordinate Wnt/β-catenin signaling to regulate cell proliferation

The canonical Wnt/β-catenin signaling pathway plays an important role in regulating cell proliferation and differentiation during development, and mutations in components of Wnt/β-catenin signaling contribute to cancers (Xu et al., 2015; Yin et al., 2016; Zong et al., 2017). As some studies in cancer cell lines suggest that δ-pcdhs may act as tumor suppressors by regulating β-catenin, we determined the effects of δ-pcdh loss on canonical Wnt/β-catenin signaling. Stimulation of the Wnt/β-catenin signaling pathway results in accumulation of β-catenin, which allows it to translocate to the nucleus and associate with the transcription factor TCF/LEF to activate target genes (Clevers, 2006; Nusse and Clevers, 2017). We used droplet digital PCR (ddPCR) to quantify the transcript levels of β-catenin/TCF target genes, *axin2* and *lef1* (Figures 4A and 4B). The levels of these transcripts were normalized against the level of *gapdh*. In the case of each δ-pcdh mutant, we observed increased expression (>3-fold) of *axin2* (Figure 4A) (*axin2*: wild type, 1.0 ± 0.0, n = 3; *pcdh1a-/-*, 4.0 ± 0.86 n = 5; *pcdh7a-/-*, 5.82±0.67, n=4; *pcdh9-/-*, 4.26±0.61, n=4; *pcdh17-/-*, 5.14±0.30, n=5; *pcdh18b-/-*, 4.21±0.25, n=4; *pcdh19-/-*, 5.36±0.59, n=5) and *lef1* (Figure 4B) (*lef1*: wild type, 1.03±0.03, n=4; *pcdh1a-/-*, 4.13±0.93, n=5; *pcdh7a-/-*, 5.98±0.82, n=4; *pcdh9-/-*, 3.65±0.36, n=5; *pcdh17-/-*, 4.41±0.68, n=5; *pcdh18b-/-*, 4.08±0.25, n=4; *pcdh19-/-*, 3.68±0.37, n=5). Taken together,
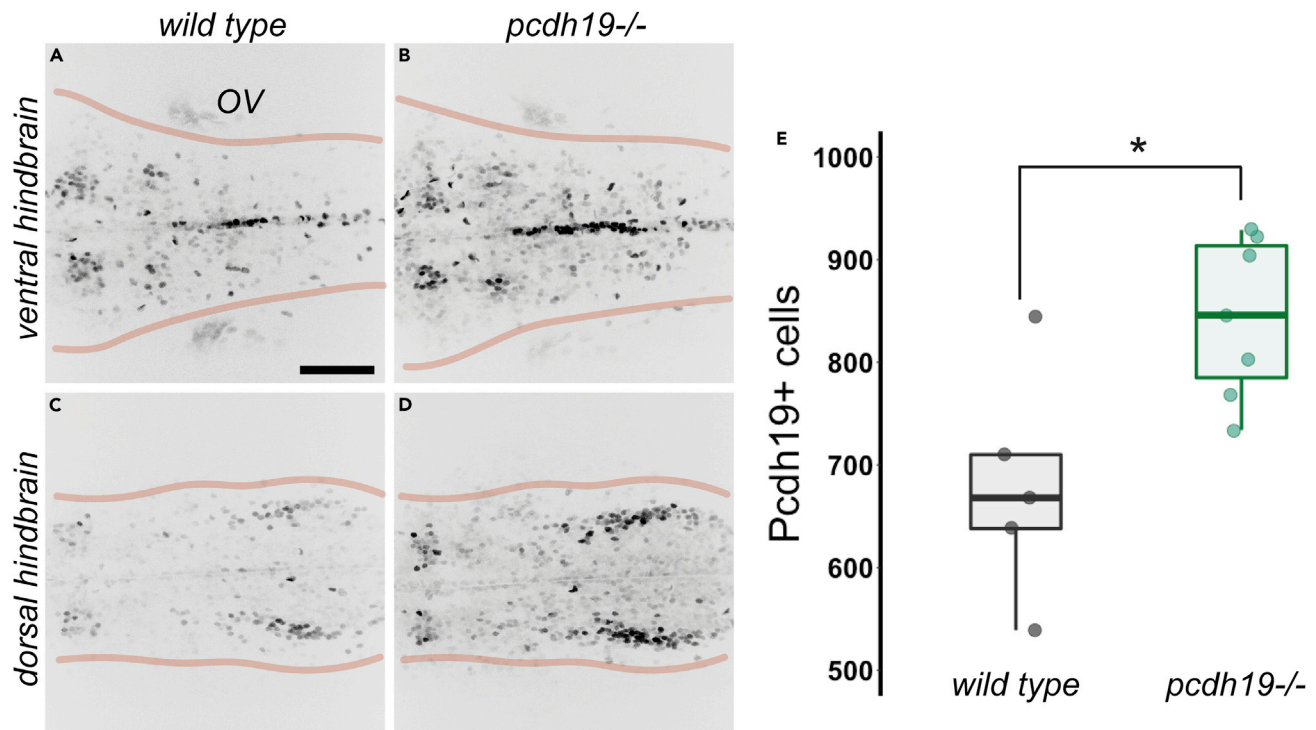
Figure 3. Increased number of pcdh19 + hindbrain neurons in pcdh19 mutants

(A and B) Maximum intensity projections of 25 optical sections spaced at 1 μm taken from the ventral hindbrains of a 3-dpf wild-type (A) or pcdh19 mutant (B) transgenic larva, expressing Histone H2A-GFP under the control of pcdh19 regulatory elements. OV, otic vesicle. Scale bar, 50 μm.

(C and D) Maximum intensity projections of 25 optical sections spaced at 1 μm taken from the dorsal hindbrains of the same wild-type (C) or pcdh19 mutant (D) transgenic larvae in (A) and (B), respectively.

(E) The pcdh19 mutants showed an elevated number of pcdh19+ cells in the hindbrains of 3-dpf TgBAC(pcdh19-0.5hsp70:H2A-GFP)[os75Tg] larvae. (WT, n = 679.8 ± 49.8 cells, n = 5; pcdh19-/-, n=843.7±29.6, n=7; *p = 0.013, two-tailed Student's t test). Error bars represent the mean +/− standard error (SEM).

these data support the idea that canonical Wnt/β-catenin signaling is elevated in the neuroepithelium of zebrafish lacking individual δ-pcdhs.

If the increased proliferation observed in δ-pcdh mutants is due to increased activation of canonical Wnt signaling, then blocking Wnt/β-catenin signaling should occlude the proliferation phenotype. To inhibit the canonical Wnt/β-catenin signaling pathway, we treated embryos with the tankyrase inhibitor XAV939 (Huang et al., 2009), which stabilizes Axin, a core component of the β-catenin destruction complex. We treated wild-type or δ-pcdh mutant embryos with XAV939 for four hours prior to fixation at 18 hpf and performed pH3 immunocytochemistry (Figure 4C). For each δ-pcdh mutant, treatment with XAV939 blocked the observed increase in cell proliferation (Figure 4C) (*wild type*, 157±5, n=25; *wild type* + XAV939, 136±2.8, n=25; *pcdh1a-/-*, 216.7±8.9, n=20; pcdh1a-/- + XAV939, 134.9±4.3, n=17; *pcdh7a-/-*, 192.9±8, n=17; pcdh7a-/- + XAV939, 143.3±3.9, n=22; pcdh9-/-, 203.6±6.9, n=16; pcdh9-/- + XAV939, 148.9±5.7, n=16; *pcdh17-/-*, 211.1±8.7, n=17; pcdh17-/- + XAV939, 141±4.9, n=18; pcdh18b-/-, 203.5±6.6, n=20; pcdh18b-/- + XAV939, 138.2±4.8, n=13; pcdh19-/-, 223.7±5.1, n=37; pcdh19-/- + XAV939, 144.3±4.8, n=19). To further probe the involvement of Wnt/β-catenin signaling in the δ-pcdh mutant phenotype, we used a dominant-negative TCF7l1a (dnTCF) (Lewis et al., 2004) to block activation of Wnt target genes (Figure 4D). A heat shock driver plasmid *pCS2-hsp70:Gal4-VP16* was co-injected with *pIScel-5xUAS:dnTCF-HA* into wild-type and δ-pcdh mutant embryos at the one-cell stage, and embryos were heat shocked (hs) at 37°C from 14–15 hpf, then fixed at 18 hpf. Injected embryos that were not heat shocked were used as controls. Expression of dnTCF was verified with anti-HA immunocytochemistry. Expression of dnTCF blocked the increased cell proliferation in the hindbrains of *pcdh1a* or *pcdh17* mutants (Figure 4D) (*pcdh1a-/- no hs*, 202.2±6.4, n=15; *pcdh1a-/- +hs*, 150.2±2.9, n=38; *pcdh17-/- no hs*, 204.1±7.2, n=17; *pcdh17-/- +hs*, 165.2±5.3, n=28). The results of treatment with XAV939 and expression
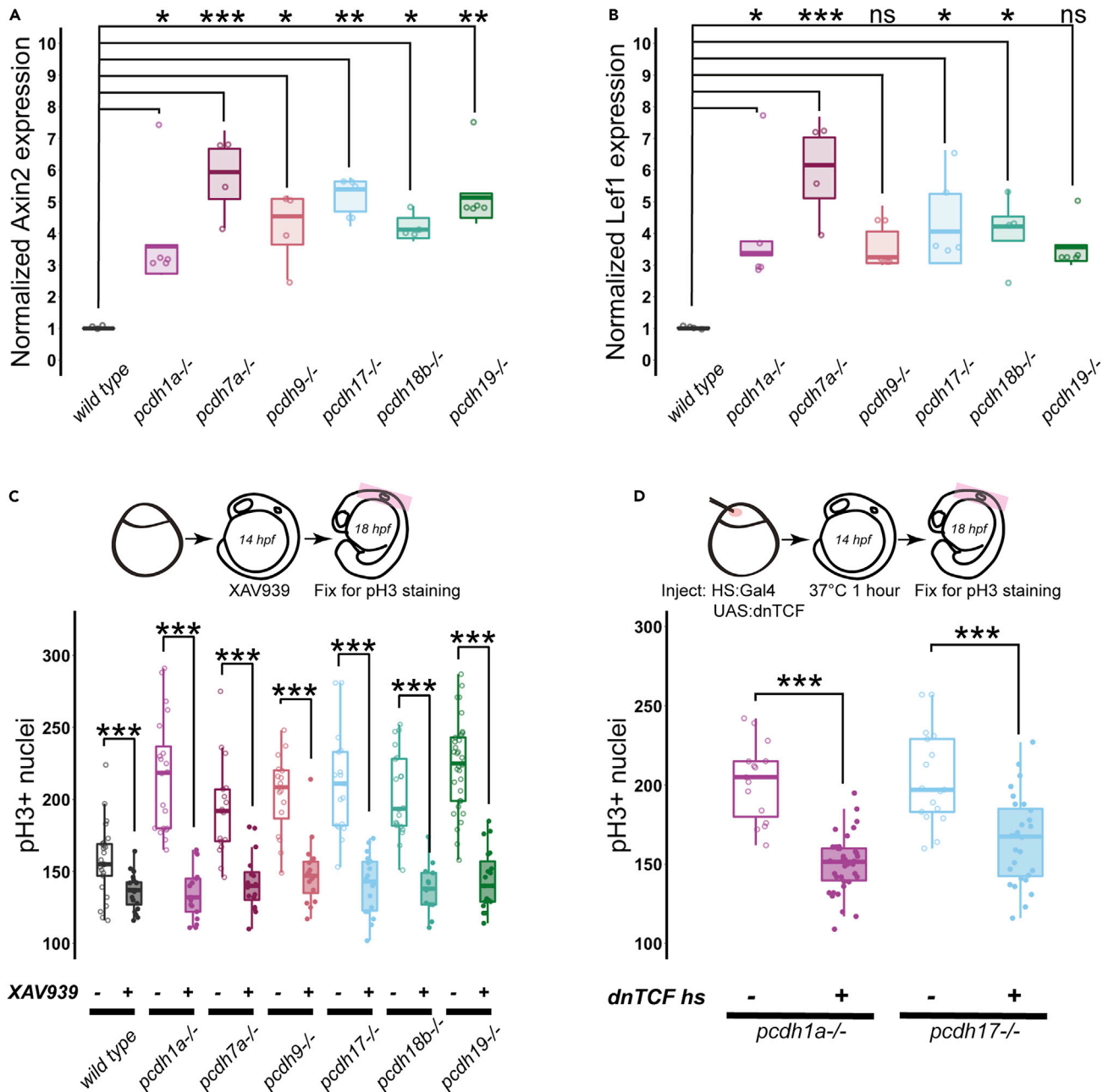
Figure 4. The δ-pcdhs coordinate Wnt/β-catenin signaling to regulate cell proliferation

(A and B) The expressions of Wnt/β-catenin target genes axin2 (A) and lef1 (B) are elevated >2-fold in each of the δ-pcdh mutants. At least three biological replicates were collected for each genotype. Expression was normalized against gapdh. Expression of axin2 or lef1 in each δ-pcdh line was normalized against the average levels in wild-type embryos. (A; axin2; WT, n = 3; pcdh1a-/-, n = 5, *p = 0.0373; pcdh7a-/-, n=4, ***p=0.0005; pcdh9-/-, n=4, *p=0.0321; pcdh17-/-, n=5, **p=0.0019; pcdh18b-/-, n=4, *p=0.0311; pcdh19-/-, n=5, **p=0.0011, one-way ANOVA with Tukey HSD). (B; lef1; WT, n=4; pcdh1a-/-, n=5, *p=0.0271; pcdh7a-/-, n=4, ***p=0.0003; pcdh9-/-, n=5, p=0.0865; pcdh17-/-, n=5, *p=0.0128; pcdh18b-/-, n=4, *p=0.0453; pcdh19-/-, n=5, p=0.0817, one-way ANOVA with Tukey HSD). Error bars represent the mean +/- standard error (SEM).

(C) To assess the role of Wnt/β-catenin signaling, embryos were soaked in 15 μM XAV939, a tankyrase inhibitor that stabilizes axin and inhibits Wnt/β-catenin signaling. In each δ-pcdh mutant, XAV939 eliminates the increased proliferation observed in the mutants. (WT, n=21; wild-type +XAV939, n=25, ***p=0.001; pcdh1a-/-, n=20; pcdh1a-/- +XAV939, n=23, ***p<0.0001; pcdh7a-/-, n=17; pcdh7a-/- +XAV939, n=22, ***p<0.0001; pcdh9-/-, n=16; pcdh9-/- +XAV939, n=16, ***p<0.0001; pcdh17-/-, n=17; pcdh17-/- +XAV939, n=18, ***p<0.0001; pcdh18b-/-, n=20; pcdh18b-/- +XAV939, n=13, ***p<0.0001; pcdh19-/-, n=38; pcdh19-/- +XAV939, n=19, ***p<0.0001, one-way ANOVA with Tukey HSD). Error bars represent the mean +/- standard error (SEM).

Figure 4. Continued

(D) As an alternative approach to blocking Wnt/β-catenin signaling, a dominant-negative TCF (dnTCF) was expressed, in which the amino-terminal β-catenin-binding domain was replaced with an HA epitope tag. Injected, un-heat shocked embryos were used as controls. When expressed in either pcdh1a (a δ1-pcdh) or pcdh17 (a δ2-pcdh) mutants, dnTCF eliminated the increased proliferation that occurs in δ-pcdh mutants (pcdh1a-/- noHS, n=15; pcdh1a-/- +HS, n=38, ***p<0.0001; pcdh17-/- noHS, n=17; pcdh17-/- +HS, n=28, ***p<0.0001, two-tailed Student's t test). Error bars represent the mean +/- standard error (SEM).

of dnTCF are consistent with the conclusion that the enhanced proliferation in δ-pcdh mutants is due to elevated Wnt/β-catenin signaling.

The δ-pcdhs interact with the Wnt receptor Ryk

Our data support the idea that the δ-pcdhs negatively regulate the canonical Wnt/β-catenin signaling pathway in the zebrafish neuroepithelium. The non-canonical Wnt receptor Ryk is a single-pass transmembrane protein with an extracellular WIF domain and a non-catalytic intracellular kinase domain (Hovens et al., 1992; Lu et al., 2004). Ryk contributes to axon guidance (Bonkowsky et al., 1999; Callahan et al., 1995; Li et al., 2009; Schmitt et al., 2006) and has been shown to be required for canonical Wnt/β-catenin signaling in HEK293T cells (Berndt et al., 2011; Lu et al., 2004). In addition, a proteomics study found several protocadherins to be part of the Ryk interactome (Berndt et al., 2011). To verify the interaction between Ryk and δ-pcdhs, we performed coimmunoprecipitation (coIP) with extracts of HEK293 cells that had been co-transfected with zebrafish Pcdh18b-GFP and zebrafish Ryk-HA (Figure 5A). In contrast, Ryk-HA did not coimmunoprecipitate with CD4-GFP, a non-specific transmembrane protein (Figure 5B). To verify the interaction between Ryk and a δ-pcdh *in vivo*, we used heat shock plasmids to drive expression of an HA epitope-tagged Ryk (Ryk-HA) and prepared protein extracts from 18-hpf zebrafish embryos. We previously generated a polyclonal antibody against the intracellular domain of Pcdh19 (Cooper et al., 2015; Emond et al., 2009). When Ryk-HA was immunoprecipitated with anti-HA antibodies, we found that endogenous Pcdh19 was also pulled down (Figure 5C). To determine whether this interaction extended to other δ-pcdh family members, we co-transfected HEK293 cells with Ryk-HA and GFP-tagged δ-pcdhs lacking their intracellular domains (Pcdh1aΔCP, Pcdh9ΔCP, Pcdh17ΔCP, and Pcdh18bΔCP). For some of the δ-pcdhs, removing the intracellular domain improves their expression and increases their localization to the cell surface. In each case, the truncated δ-pcdhs coimmunoprecipitated with Ryk-HA (Figure 5D), supporting the conclusion that Ryk can exist in complex with δ-pcdhs. When co-transfected into the ZF4 zebrafish cell line, Pcdh19-GFP and Ryk-HA colocalized both on the cell surface and in intracellular puncta (Figure 5E). Together, these data support the idea that δ-pcdh family members interact with Ryk and colocalize in cells, both on the cell surface and in intracellular compartments.

Ryk promotes Wnt/β-catenin signaling and is required for increased cell proliferation in δ-pcdh mutants

Based on the close association of the δ-pcdhs with Ryk, both *in vitro* and *in vivo*, we hypothesized that Ryk was required for the enhanced proliferation observed in δ-pcdh mutants. To investigate the role of Ryk in the neuroepithelium, we used CRISPR-Cas9 to generate a mutant zebrafish line lacking Ryk. Targeting a site near the amino terminus of zebrafish *ryk*, we obtained the frameshift allele, *ryk(Δ-19)* (Figure 6A). To determine the effect of Ryk loss on neural progenitor cell proliferation, we performed whole-mount immunocytochemistry with antibodies against pH3 in the hindbrain at 18 hpf in *ryk* mutants and in embryos injected with *ryk* gRNA and Cas9 mRNA. The *ryk* gRNA is highly efficient and works effectively as a knockdown reagent. In both cases, loss of Ryk resulted in a modest reduction in proliferation (Figures 6B and 6C; *wild type*, n = 25, 157.6 ± 5; *ryk-/-*, n=14, 139.4±7; *ryk*CRISPR, n=26, 143.3±6.8) that was not statistically significant. As prior studies have suggested that Ryk is required for canonical Wnt/β-catenin signaling *in vitro*, we used ddPCR to determine the effects of Ryk loss on the levels of the β-catenin/TCF target genes, *axin2* and *lef1* (Figures 6D and 6E). We found that the Wnt/β-catenin pathway was slightly suppressed in *ryk* mutant embryos and in embryos injected with CRISPR-Cas9 directed against *ryk* (Figures 6D and 6E) (*axin2*: wt, 1.0±0.13, n=3; *ryk-/-*, 0.64±0.04, n=3; *ryk*CRISPR, 0.86±0.03, n=3; *lef1*: wt, 1.0±0.06, n=3; *ryk-/-*, 0.58±0.09, n=3; *ryk*CRISPR, 0.58±0.09, n=3). This is consistent with Ryk participating in canonical Wnt signaling in the developing zebrafish neuroepithelium.

The loss of δ-pcdhs leads to enhanced Wnt/β-catenin signaling and cell proliferation (Figure 4). In contrast, the loss of Ryk results in reduced Wnt/β-catenin signaling and cell proliferation (Figures 6D and 6E). As we show that Ryk can exist in a complex with δ-pcdhs (Figure 5), we hypothesized that Ryk might be required
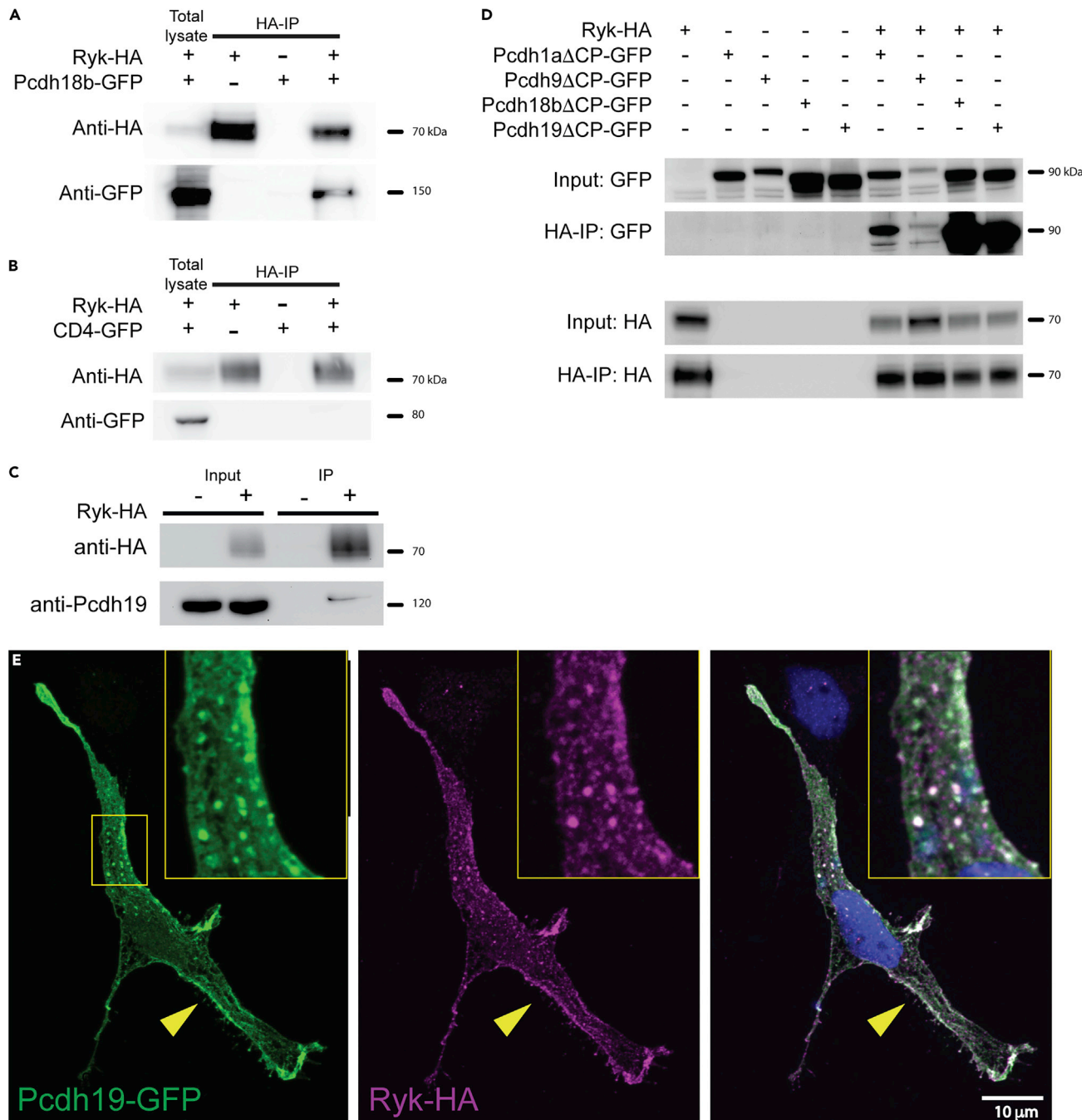
Figure 5. The δ-pcdhs interact with the Wnt receptor Ryk

(A) When co-transfected into HEK293 cells, zebrafish Ryk-HA is able to coimmunoprecipitate Pcdh18b-GFP.

(B) Ryk-HA does not coimmunoprecipitate with CD4-GFP.

(C) To verify that δ-pcdhs interact with Ryk *in vivo*, an epitope-tagged Ryk (Ryk-HA) was expressed in 18 hpf embryos and immunoprecipitated from embryo extracts. Western blots show that endogenous Pcdh19 coimmunoprecipitates with Ryk-HA *in vivo*.

(D) Ryk-HA is able to coimmunoprecipitate δ1-pcdh (Pcdh1a or Pcdh9) or δ2-pcdh (Pcdh18b or Pcdh19) family members. To improve expression of some δ-pcdhs, we generated constructs lacking most of their intracellular domains (ΔCP). Thus, the intracellular domains are dispensable for interacting with Ryk.

(E) Pcdh19-GFP (green) and Ryk-HA (magenta) were co-transfected in the zebrafish ZF4 cell line. Pcdh19 and Ryk co-localize, both on the cell surface (yellow arrowhead), including membrane protrusions, and in intracellular puncta (inset). Scale bar = 10 μm.

Figure 6. Ryk promotes Wnt/β-catenin signaling and is required for increased cell proliferation in δ-pcdh mutants

(A) CRISPR-Cas9 was used to generate indel mutations in zebrafish ryk. The selected target site (red text) was within the sequence encoding the signal peptide.

Figure 6. *Continued*

(B and C) Loss of ryk shows a modest decrease in pH3 labeling in 18-hpf zebrafish embryos. In addition to being used for generating germline lesions in ryk, the gRNA directed against ryk is a very effective knockdown reagent, as verified by HRMA analysis. Both ryk mutants and ryk CRISPR-injected embryos showed a modest decrease in pH3 labeling (*wild type*, n = 25, 157.6 $\pm$ 5; *ryk-/-*, n=14, 139.4$\pm$7; *ryk*CRISPR, n=26, 143.3$\pm$6.8), which was not statistically significant by one-way ANOVA with Tukey HSD.

(D and E) Loss or reduction of ryk leads to reduced levels of the Wnt/β-catenin target genes axin2 (D) and lef1 (E) as determined by ddPCR, suggesting that Ryk promotes canonical Wnt signaling. (axin2: WT versus ryk-/-, n=3, *p=0.0479; axin2: WT versus ryk CRISPR, n=3, p=0.4802; lef1: WT versus ryk-/-, n=3, *p=0.0241; lef1: WT versus ryk CRISPR, n=3, *p=0.0246, one-way ANOVA with Tukey HSD). Error bars represent the mean +/- standard error (SEM).

(F) CRISPR-Cas9 was used to knockdown Ryk expression in each of the δ-pcdh mutant lines. Reduction of Ryk in the mutant backgrounds eliminated the increased pH3 labeling, suggesting that the presence of Ryk is required for the increased proliferation in these lines. (pcdh1a-/-, n=20; pcdh1a-/- +rykCRISPR, n=23, ***p<0.0001; pcdh7a-/-, n=17; pcdh7a-/- + rykCRISPR, n=21, ***p<0.0001; pcdh9-/-, n=16; pcdh9-/- + rykCRISPR, n=15, ***p<0.0001; pcdh17-/-, n=17; pcdh17-/- + rykCRISPR, n=21, ***p<0.0001; pcdh18b-/-, n=20; pcdh18b-/- + rykCRISPR, n=14, ***p<0.0001; pcdh19-/-, n=38; pcdh19-/- + rykCRISPR, n=19, ***p<0.0001, one-way ANOVA with Tukey HSD). Error bars represent the mean +/- standard error (SEM).

(G) Knockdown of pcdh19 using CRISPR-Cas9 causes an elevation of pH3 labeling in wild-type embryos (*wild type*, 122.4$\pm$6.1, n=14; *wild type* + *pcdh19*CRISPR, 203.0$\pm$10.5, n=20, ***p<0.0001, two-tailed Student's t test). In contrast, pcdh19 knockdown does not cause increased pH3 labeling in ryk-/- mutants (*ryk$^{-/-}$*, 136.8$\pm$5.3, n=18; *ryk$^{-/-}$* + *pcdh19*CRISPR, 125.5$\pm$3.2, n=21, p=0.0692, two-tailed Student's t test). Error bars represent the mean +/- standard error (SEM).

for the δ-pcdh phenotype. To test this, we used CRISPR-Cas9 injection to knockdown Ryk in δ-pcdh mutant embryos (Figure 6F). In each case, knockdown of Ryk blocked the increased proliferation observed in δ-pcdh mutants (Figure 6F; *pcdh1a-/-*, 216.7 $\pm$ 8.9, n = 20; *pcdh1a-/- +ryk*CRISPR, 144.6$\pm$3.4, n=23; *pcdh7a-/-*, 192.9$\pm$8, n=17; *pcdh7a-/- + ryk*CRISPR, 144.6$\pm$3.9, n=21; *pcdh9-/-*, 203.6$\pm$6.9, n=16; *pcdh9-/- + ryk*CRISPR, 164.3$\pm$6.5, n=15; *pcdh17-/-*, 211.1$\pm$8.7, n=17; *pcdh17-/- + ryk*CRISPR, 186.3$\pm$6.5, n=21; *pcdh18b-/-*, 203.5$\pm$6.6, n=20; *pcdh18b-/- + ryk*CRISPR, 153.2$\pm$3, n=14; *pcdh19-/-*, 223.7$\pm$5, n=38; *pcdh19-/- + ryk*CRISPR, 160.5$\pm$10, n=19). As a further test of the role of Ryk, we identified a highly efficient gRNA against *pcdh19*. When injected into wild-type embryos, Cas9/*pcdh19*CRISPR led to an increase of pH3+ nuclei, similar to what we observed in *pcdh19* mutants, yet failed to elicit a similar response when injected into *ryk* mutants (Figure 6G; *wild type*, 122.4$\pm$6.1, n=14; *wild type* + *pcdh19*CRISPR, 203.0$\pm$10.5, n=20; *ryk$^{-/-}$*, 136.8$\pm$5.3, n=18; *ryk$^{-/-}$* + *pcdh19*CRISPR, 125.5$\pm$3.2, n=21). Thus, the presence of Ryk is required for the loss of δ-pcdhs to elicit an effect on proliferation. As Ryk participates in the canonical Wnt/β-catenin pathway, we speculate that (1) δ-pcdhs negatively regulate Ryk, possibly by influencing its trafficking or stability, and (2) the increased Wnt/β-catenin signaling observed in δ-pcdh mutants is due to disinhibition of Ryk.

DISCUSSION

We previously showed that zebrafish *pcdh19* is expressed in a subset of neural progenitor cells within the optic tectum and that cell divisions of these progenitors give rise to radial columns of sibling neurons that share the expression of *pcdh19* (Cooper et al., 2015). Other evidence supports the observation that δ-pcdhs are expressed in neural progenitor cells (Bergsland et al., 2011; McAninch and Thomas, 2014) and that they regulate neurogenesis (Fujitani et al., 2016; Homan et al., 2018; Zhang et al., 2014). Here, we show that the loss of individual δ-pcdh family members leads to an increase in the division of neural progenitor cells and neurogenesis and that they likely do so through an increase in Wnt/β-catenin signaling. It is not presently clear whether the increase in cell divisions observed in δ-pcdh mutants is due to an expansion of the progenitor pool through symmetric cell divisions, premature neurogenic divisions, or both. The increased number of neurons expressing a *pcdh19* reporter in *pcdh19$^{-/-}$* embryos could be consistent with either scenario, and further work will be required to settle this issue. As δ-pcdhs exhibit distinct regional expression in the nervous system (Blevins et al., 2011; Kim et al., 2007), and may define distinct cell lineages within a brain region (Cooper et al., 2015), the δ-pcdhs could provide a mechanism to differentially modulate cell responsiveness to canonical Wnt signaling within populations of progenitors. As δ-pcdhs have been proposed to contribute to a molecular code for cellular identity in the development of neural circuits (Bisogni et al., 2018; Harrison et al., 2020), our results suggest that this role could originate at the level of neural progenitor cells. It remains to be shown whether individual δ-pcdhs define distinct lineages or whether they define a combinatorial code. Our data further indicate that the δ-pcdhs interact with canonical Wnt signaling through the receptor Ryk, as Ryk is required for the elevated pH3 labeling observed in δ-pcdh mutants. Although Ryk has also previously been linked to Wnt/β-catenin signaling *in vitro*, the mechanism by which Ryk facilitates Wnt/β-catenin signaling and promotes cell division remains to be elucidated. Overall, our results are consistent with δ-pcdhs acting as unexpected and novel upstream regulators of canonical Wnt signaling and provide insight into the contributions of both δ-pcdhs (Hirano and Takeichi, 2012;

Redies et al., 2012) and Wnt/β-catenin signaling (De Ferrari and Moon, 2006; Kwan et al., 2016) to neuro-developmental disorders and to cancer (Berx and van Roy, 2009; Polakis, 2012; van Roy, 2014; Zhan et al., 2017).

Limitations of the study

We have shown that the δ-pcdhs regulate proliferation of neural progenitor cells, but the precise molecular mechanisms remain uncertain. The mechanism by which the δ-pcdhs interact with and regulate Ryk and how Ryk influences Wnt/β-catenin signaling are unclear.

STAR★METHODS

Detailed methods are provided in the online version of this paper and include the following:

- KEY RESOURCES TABLE
- RESOURCE AVAILABILITY
  ○ Lead contact
  ○ Materials availability
  ○ Data and code availability
- EXPERIMENTAL MODEL AND SUBJECT DETAILS
  ○ Zebrafish maintenance
- METHOD DETAILS
  ○ TALEN/CRISPR production of germline lesions
  ○ BAC recombineering and transgenesis
  ○ Phylogenetic analysis
  ○ Whole mount *in situ* hybridization
  ○ Coimmunoprecipitation and western blotting
  ○ ZF4 cell culture and immunocytochemistry
  ○ axin2 and lef1 transcript quantification
  ○ Immunocytochemistry and two-photon imaging
  ○ Image analysis and cell counting
  ○ Timelapse imaging and analysis of M phase
- QUANTIFICATION AND STATISTICAL ANALYSIS

SUPPLEMENTAL INFORMATION

Supplemental information can be found online at https://doi.org/10.1016/j.isci.2021.102932.

AUTHOR CONTRIBUTIONS

S.B. performed experiments, analyzed data, made figures and wrote/edited manuscript. M.R.E. performed experiments, analyzed data, made figures, and wrote/edited manuscript. K.P.C. analyzed data. J.D.J. conceived project, designed experiments, made figures, and wrote/edited manuscript.

DECLARATION OF INTERESTS

The authors declare no competing interests.

REFERENCES

Aamar, E., and Dawid, I.B. (2008). Protocadherin-18a has a role in cell adhesion, behavior and migration in zebrafish development. Dev. Biol. *318*, 335–346. https://doi.org/10.1016/j.ydbio.2008.03.040.

Bedell, V.M., Wang, Y., Campbell, J.M., Poshusta, T.L., Starker, C.G., Krug, R.G., 2nd, Tan, W., Penheiter, S.G., Ma, A.C., Leung, A.Y., et al. (2012). In vivo genome editing using a high-efficiency TALEN system. Nature *491*, 114–118. https://doi.org/10.1038/nature11537.

Bergsland, M., Ramskold, D., Zaouter, C., Klum, S., Sandberg, R., and Muhr, J. (2011). Sequentially acting Sox transcription factors in neural lineage development. Genes Dev. *25*, 2453–2464. https://doi.org/10.1101/gad.176008.111.

Berndt, J.D., Aoyagi, A., Yang, P., Anastas, J.N., Tang, L., and Moon, R.T. (2011). Mindbomb 1, an E3 ubiquitin ligase, forms a complex with RYK to activate Wnt/beta-catenin signaling. J. Cell Biol. *194*, 737–750. https://doi.org/10.1083/jcb.201107021.

Berx, G., and van Roy, F. (2009). Involvement of members of the cadherin superfamily in cancer. Cold Spring Harb. Perspect. Biol. *1*, a003129. https://doi.org/10.1101/cshperspect.a003129.

Bing, Y., Tian, M., Li, G., Jiang, B., Ma, Z., Li, L., Wang, L., Wang, H., and Xiu, D. (2018). Down-regulated of PCDH10 predicts poor prognosis in hepatocellular carcinoma patients. Medicine (Baltimore) *97*, e12055. https://doi.org/10.1097/MD.0000000000012055.

Bisogni, A.J., Ghazanfar, S., Williams, E.O., Marsh, H.M., Yang, J.Y., and Lin, D.M. (2018). Tuning of delta-protocadherin adhesion through combinatorial diversity. Elife *7*. https://doi.org/10.7554/eLife.41050.

Biswas, S., Emond, M.R., Duy, P.Q., Hao le, T., Beattie, C.E., and Jontes, J.D. (2014). Protocadherin-18b interacts with Nap1 to control motor axon growth and arborization in zebrafish. Mol. Biol. Cell *25*, 633–642. https://doi.org/10.1091/mbc.E13-08-0475.

Biswas, S., Emond, M.R., and Jontes, J.D. (2010). Protocadherin-19 and N-cadherin interact to control cell movements during anterior neurulation. J. Cell Biol. *191*, 1029–1041. https://doi.org/10.1083/jcb.201007008.

Blevins, C.J., Emond, M.R., Biswas, S., and Jontes, J.D. (2011). Differential expression, alternative splicing, and adhesive properties of the zebrafish delta1-protocadherins. Neuroscience *199*, 523–534. https://doi.org/10.1016/j.neuroscience.2011.09.061.

Bonkowsky, J.L., Yoshikawa, S., O'Keefe, D.D., Scully, A.L., and Thomas, J.B. (1999). Axon routing across the midline controlled by the Drosophila Derailed receptor. Nature *402*, 540–544. https://doi.org/10.1038/990122.

Bruining, H., Matsui, A., Oguro-Ando, A., Kahn, R.S., Van't Spijker, H.M., Akkermans, G., Stiedl, O., van Engeland, H., Koopmans, B., van Lith, H.A., et al. (2015). Genetic mapping in mice reveals the involvement of Pcdh9 in long-term social and object recognition and sensorimotor development. Biol. Psychiatry *78*, 485–495. https://doi.org/10.1016/j.biopsych.2015.01.017.

Cadigan, K.M., and Liu, Y.I. (2006). Wnt signaling: complexity at the surface. J. Cell Sci. *119*, 395–402. https://doi.org/10.1242/jcs.02826.

Callahan, C.A., Muralidhar, M.G., Lundgren, S.E., Scully, A.L., and Thomas, J.B. (1995). Control of neuronal pathway selection by a Drosophila receptor protein-tyrosine kinase family member. Nature *376*, 171–174. https://doi.org/10.1038/376171a0.

Cermak, T., Doyle, E.L., Christian, M., Wang, L., Zhang, Y., Schmidt, C., Baller, J.A., Somia, N.V., Bogdanove, A.J., and Voytas, D.F. (2011). Efficient design and assembly of custom TALEN and other TAL effector-based constructs for DNA targeting. Nucleic Acids Res. *39*, e82. https://doi.org/10.1093/nar/gkr218.

Chen, X., and Gumbiner, B.M. (2006). Paraxial protocadherin mediates cell sorting and tissue morphogenesis by regulating C-cadherin adhesion activity. J. Cell Biol. *174*, 301–313. https://doi.org/10.1083/jcb.200602062.

Clevers, H. (2006). Wnt/beta-catenin signaling in development and disease. Cell *127*, 469–480. https://doi.org/10.1016/j.cell.2006.10.018.

Cooper, S.R., Emond, M.R., Duy, P.Q., Liebau, B.G., Wolman, M.A., and Jontes, J.D. (2015). Protocadherins control the modular assembly of neuronal columns in the zebrafish optic tectum. J. Cell Biol. *211*, 807–814. https://doi.org/10.1083/jcb.201507108.

Cooper, S.R., Jontes, J.D., and Sotomayor, M. (2016). Structural determinants of adhesion by Protocadherin-19 and implications for its role in epilepsy. Elife *5*. https://doi.org/10.7554/eLife.18529.

Dahlem, T.J., Hoshijima, K., Jurynec, M.J., Gunther, D., Starker, C.G., Locke, A.S., Weis, A.M., Voytas, D.F., and Grunwald, D.J. (2012). Simple methods for generating and detecting locus-specific mutations induced with TALENs in the zebrafish genome. PLoS Genet. *8*, e1002861. https://doi.org/10.1371/journal.pgen.1002861.

De Ferrari, G.V., and Moon, R.T. (2006). The ups and downs of Wnt signaling in prevalent neurological disorders. Oncogene *25*, 7545–7553. https://doi.org/10.1038/sj.onc.1210064.

Depienne, C., Bouteiller, D., Keren, B., Cheuret, E., Poirier, K., Trouillard, O., Benyahia, B., Quelin, C., Carpentier, W., Julia, S., et al. (2009). Sporadic infantile epileptic encephalopathy caused by mutations in PCDH19 resembles Dravet syndrome but mainly affects females. PLoS Genet. *5*, e1000381. https://doi.org/10.1371/journal.pgen.1000381.

Depienne, C., and LeGuern, E. (2012). PCDH19-related infantile epileptic encephalopathy: an unusual X-linked inheritance disorder. Hum. Mutat. *33*, 627–634. https://doi.org/10.1002/humu.22029.

Dibbens, L.M., Tarpey, P.S., Hynes, K., Bayly, M.A., Scheffer, I.E., Smith, R., Bomar, J., Sutton, E., Vandeleur, L., Shoubridge, C., et al. (2008). X-linked protocadherin 19 mutations cause female-limited epilepsy and cognitive impairment. Nat. Genet. *40*, 776–781. https://doi.org/10.1038/ng.149.

Emond, M.R., Biswas, S., and Jontes, J.D. (2009). Protocadherin-19 is essential for early steps in brain morphogenesis. Dev. Biol. *334*, 72–83. https://doi.org/10.1016/j.ydbio.2009.07.008.

Fujitani, M., Zhang, S., Fujiki, R., Fujihara, Y., and Yamashita, T. (2016). A chromosome 16p13.11 microduplication causes hyperactivity through dysregulation of miR-484/protocadherin-19 signaling. Mol. Psychiatry. https://doi.org/10.1038/mp.2016.106.

Harrison, O.J., Brasch, J., Katsamba, P.S., Ahlsen, G., Noble, A.J., Dan, H., Sampogna, R.V., Potter, C.S., Carragher, B., Honig, B., and Shapiro, L. (2020). Family-wide structural and biophysical analysis of binding interactions among non-clustered delta-protocadherins. Cell Rep. *30*, 2655–2671 e2657. https://doi.org/10.1016/j.celrep.2020.02.003.

Hayashi, S., Inoue, Y., Kiyonari, H., Abe, T., Misaki, K., Moriguchi, H., Tanaka, Y., and Takeichi, M. (2014). Protocadherin-17 mediates collective axon extension by recruiting actin regulator complexes to interaxonal contacts. Dev. Cell *30*, 673–687. https://doi.org/10.1016/j.devcel.2014.07.015.

Hirano, S., and Takeichi, M. (2012). Cadherins in brain morphogenesis and wiring. Physiol. Rev. *92*, 597–634. https://doi.org/10.1152/physrev.00014.2011.

Homan, C.C., Pederson, S., To, T.H., Tan, C., Piltz, S., Corbett, M.A., Wolvetang, E., Thomas, P.Q., Jolly, L.A., and Gecz, J. (2018). PCDH19 regulation of neural progenitor cell differentiation suggests asynchrony of neurogenesis as a mechanism contributing to PCDH19 Girls Clustering Epilepsy. Neurobiol. Dis. *116*, 106–119. https://doi.org/10.1016/j.nbd.2018.05.004.

Hovens, C.M., Stacker, S.A., Andres, A.C., Harpur, A.G., Ziemiecki, A., and Wilks, A.F. (1992). RYK, a receptor tyrosine kinase-related molecule with unusual kinase domain motifs. Proc. Natl. Acad. Sci. U S A *89*, 11818–11822. https://doi.org/10.1073/pnas.89.24.11818.

Huang, S.M., Mishina, Y.M., Liu, S., Cheung, A., Stegmeier, F., Michaud, G.A., Charlat, O., Wiellette, E., Zhang, Y., Wiessner, S., et al. (2009). Tankyrase inhibition stabilizes axin and antagonizes Wnt signalling. Nature *461*, 614–620. https://doi.org/10.1038/nature08356.

Hulpiau, P., and van Roy, F. (2011). New insights into the evolution of metazoan cadherins. Mol. Biol. Evol. *28*, 647–657. https://doi.org/10.1093/molbev/msq233.

Hwang, W.Y., Fu, Y., Reyon, D., Maeder, M.L., Tsai, S.Q., Sander, J.D., Peterson, R.T., Yeh, J.R., and Joung, J.K. (2013). Efficient genome editing in zebrafish using a CRISPR-Cas system. Nat.

Biotechnol. *31*, 227–229. https://doi.org/10.1038/nbt.2501.

Jao, L.E., Wente, S.R., and Chen, W. (2013). Efficient multiplex biallelic zebrafish genome editing using a CRISPR nuclease system. Proc. Natl. Acad. Sci. U S A *110*, 13904–13909. https://doi.org/10.1073/pnas.1308335110.

Kim, S.H., Yamamoto, A., Bouwmeester, T., Agius, E., and Robertis, E.M. (1998). The role of paraxial protocadherin in selective adhesion and cell movements of the mesoderm during Xenopus gastrulation. Development *125*, 4681–4690.

Kim, S.Y., Chung, H.S., Sun, W., and Kim, H. (2007). Spatiotemporal expression pattern of non-clustered protocadherin family members in the developing rat brain. Neuroscience *147*, 996–1021. https://doi.org/10.1016/j.neuroscience.2007.03.052.

Kraft, B., Berger, C.D., Wallkamm, V., Steinbeisser, H., and Wedlich, D. (2012). Wnt-11 and Fz7 reduce cell adhesion in convergent extension by sequestration of PAPC and C-cadherin. J. Cell Biol. *198*, 695–709. https://doi.org/10.1083/jcb.201110076.

Kwan, V., Unda, B.K., and Singh, K.K. (2016). Wnt signaling networks in autism spectrum disorder and intellectual disability. J. Neurodev. Disord. *8*, 45. https://doi.org/10.1186/s11689-016-9176-3.

Lal, D., Ruppert, A.K., Trucks, H., Schulz, H., de Kovel, C.G., Kasteleijn-Nolst Trenite, D., Sonsma, A.C., Koeleman, B.P., Lindhout, D., Weber, Y.G., et al. (2015). Burden analysis of rare microdeletions suggests a strong impact of neurodevelopmental genes in genetic generalised epilepsies. PLoS Genet. *11*, e1005226. https://doi.org/10.1371/journal.pgen.1005226.

Leung, L., Klopper, A.V., Grill, S.W., Harris, W.A., and Norden, C. (2011). Apical migration of nuclei during G2 is a prerequisite for all nuclear motion in zebrafish neuroepithelia. Development *138*, 5003–5013. https://doi.org/10.1242/dev.071522.

Leung, L.C., Urbancic, V., Baudet, M.L., Dwivedy, A., Bayley, T.G., Lee, A.C., Harris, W.A., and Holt, C.E. (2013). Coupling of NF-protocadherin signaling to axon guidance by cue-induced translation. Nat. Neurosci. *16*, 166–173. https://doi.org/10.1038/nn.3290.

Lewis, J.L., Bonner, J., Modrell, M., Ragland, J.W., Moon, R.T., Dorsky, R.I., and Raible, D.W. (2004). Reiterated Wnt signaling during zebrafish neural crest development. Development *131*, 1299–1308. https://doi.org/10.1242/dev.01007.

Li, L., Hutchins, B.I., and Kalil, K. (2009). Wnt5a induces simultaneous cortical axon outgrowth and repulsive axon guidance through distinct signaling mechanisms. J. Neurosci. *29*, 5873–5883. https://doi.org/10.1523/JNEUROSCI.0183-09.2009.

Light, S.E.W., and Jontes, J.D. (2019). Multiplane calcium imaging reveals disrupted development of network topology in zebrafish pcdh19 mutants. eNeuro *6*. https://doi.org/10.1523/ENEURO.0420-18.2019.

Lin, Y., Ge, X., Zhang, X., Wu, Z., Liu, K., Lin, F., Dai, C., Guo, W., and Li, J. (2018). Protocadherin-8 promotes invasion and metastasis via laminin subunit gamma2 in gastric cancer. Cancer Sci. *109*, 732–740. https://doi.org/10.1111/cas.13502.

Lu, W., Yamamoto, V., Ortega, B., and Baltimore, D. (2004). Mammalian Ryk is a Wnt coreceptor required for stimulation of neurite outgrowth. Cell *119*, 97–108. https://doi.org/10.1016/j.cell.2004.09.019.

MacDonald, B.T., Tamai, K., and He, X. (2009). Wnt/beta-catenin signaling: components, mechanisms, and diseases. Dev. Cell *17*, 9–26. https://doi.org/10.1016/j.devcel.2009.06.016.

Mah, K.M., Houston, D.W., and Weiner, J.A. (2016). The gamma-Protocadherin-C3 isoform inhibits canonical Wnt signalling by binding to and stabilizing Axin1 at the membrane. Sci. Rep. *6*, 31665. https://doi.org/10.1038/srep31665.

McAninch, D., and Thomas, P. (2014). Identification of highly conserved putative developmental enhancers bound by SOX3 in neural progenitors using ChIP-Seq. PLoS One *9*, e113361. https://doi.org/10.1371/journal.pone.0113361.

Morrow, E.M., Yoo, S.Y., Flavell, S.W., Kim, T.K., Lin, Y., Hill, R.S., Mukaddes, N.M., Balkhy, S., Gascon, G., Hashmi, A., et al. (2008). Identifying autism loci and genes by tracing recent shared ancestry. Science *321*, 218–223. https://doi.org/10.1126/science.1157657.

Nusse, R., and Clevers, H. (2017). Wnt/beta-Catenin signaling, disease, and emerging therapeutic modalities. Cell *169*, 985–999. https://doi.org/10.1016/j.cell.2017.05.016.

Perez-Palma, E., Helbig, I., Klein, K.M., Anttila, V., Horn, H., Reinthaler, E.M., Gormley, P., Ganna, A., Byrnes, A., Pernhorst, K., et al. (2017). Heterogeneous contribution of microdeletions in the development of common generalised and focal epilepsies. J. Med. Genet. *54*, 598–606. https://doi.org/10.1136/jmedgenet-2016-104495.

Piper, M., Dwivedy, A., Leung, L., Bradley, R.S., and Holt, C.E. (2008). NF-protocadherin and TAF1 regulate retinal axon initiation and elongation in vivo. J. Neurosci. *28*, 100–105. https://doi.org/10.1523/JNEUROSCI.4490-07.2008.

Piton, A., Gauthier, J., Hamdan, F.F., Lafreniere, R.G., Yang, Y., Henrion, E., Laurent, S., Noreau, A., Thibodeau, P., Karemera, L., et al. (2011). Systematic resequencing of X-chromosome synaptic genes in autism spectrum disorder and schizophrenia. Mol. Psychiatry *16*, 867–880. https://doi.org/10.1038/mp.2010.54.

Polakis, P. (2012). Wnt signaling in cancer. Cold Spring Harb. Perspect. Biol. *4*. https://doi.org/10.1101/cshperspect.a008052.

Pologruto, T.A., Sabatini, B.L., and Svoboda, K. (2003). ScanImage: flexible software for operating laser scanning microscopes. Biomed. Eng. Online *2*, 13. https://doi.org/10.1186/1475-925X-2-13.

Redies, C., Hertel, N., and Hubner, C.A. (2012). Cadherins and neuropsychiatric disorders. Brain Res. *1470*, 130–144. https://doi.org/10.1016/j.brainres.2012.06.020.

Schindelin, J., Arganda-Carreras, I., Frise, E., Kaynig, V., Longair, M., Pietzsch, T., Preibisch, S., Rueden, C., Saalfeld, S., Schmid, B., et al. (2012). Fiji: an open-source platform for biological-image analysis. Nat. Methods *9*, 676–682. https://doi.org/10.1038/nmeth.2019.

Schmitt, A.M., Shi, J., Wolf, A.M., Lu, C.C., King, L.A., and Zou, Y. (2006). Wnt-Ryk signalling mediates medial-lateral retinotectal topographic mapping. Nature *439*, 31–37. https://doi.org/10.1038/nature04334.

Shihavuddin, A., Basu, S., Rexhepaj, E., Delestro, F., Menezes, N., Sigoillot, S.M., Del Nery, E., Selimi, F., Spassky, N., and Genovesio, A. (2017). Smooth 2D manifold extraction from 3D image stack. Nat. Commun. *8*, 15554. https://doi.org/10.1038/ncomms15554.

Tang, X., Yin, X., Xiang, T., Li, H., Li, F., Chen, L., and Ren, G. (2012). Protocadherin 10 is frequently downregulated by promoter methylation and functions as a tumor suppressor gene in non-small cell lung cancer. Cancer Biomark. *12*, 11–19. https://doi.org/10.3233/CBM-2012-00280.

van Roy, F. (2014). Beyond E-cadherin: roles of other cadherin superfamily members in cancer. Nat. Rev. Cancer *14*, 121–134. https://doi.org/10.1038/nrc3647.

Vanhalst, K., Kools, P., Staes, K., van Roy, F., and Redies, C. (2005). delta-Protocadherins: a gene family expressed differentially in the mouse brain. Cell. Mol. Life Sci. *62*, 1247–1259. https://doi.org/10.1007/s00018-005-5021-7.

Westerfield, M. (1995). The Zebrafish Book (University of Oregon Press).

Williams, J.S., Hsu, J.Y., Rossi, C.C., and Artinger, K.B. (2018). Requirement of zebrafish pcdh10a and pcdh10b in melanocyte precursor migration. Dev. Biol. *444*, S274–S286. https://doi.org/10.1016/j.ydbio.2018.03.022.

Wu, C., Niu, L., Yan, Z., Wang, C., Liu, N., Dai, Y., Zhang, P., and Xu, R. (2015). Pcdh11x negatively regulates dendritic branching. J. Mol. Neurosci. *56*, 822–828. https://doi.org/10.1007/s12031-015-0515-8.

Xu, Y., Yang, Z., Yuan, H., Li, Z., Li, Y., Liu, Q., and Chen, J. (2015). PCDH10 inhibits cell proliferation of multiple myeloma via the negative regulation of the Wnt/beta-catenin/BCL-9 signaling pathway. Oncol. Rep. *34*, 747–754. https://doi.org/10.3892/or.2015.4056.

Yin, X., Xiang, T., Mu, J., Mao, H., Li, L., Huang, X., Li, C., Feng, Y., Luo, X., Wei, Y., et al. (2016). Protocadherin 17 functions as a tumor suppressor suppressing Wnt/beta-catenin signaling and cell metastasis and is frequently methylated in breast cancer. Oncotarget *7*, 51720–51732. https://doi.org/10.18632/oncotarget.10102.

Zhan, T., Rindtorff, N., and Boutros, M. (2017). Wnt signaling in cancer. Oncogene *36*, 1461–1473. https://doi.org/10.1038/onc.2016.304.

Zhang, P., Wang, H., Wang, J., Liu, Q., Wang, Y., Feng, F., and Shi, L. (2017). Association between protocadherin 8 promoter hypermethylation and the pathological status of prostate cancer. Oncol. Lett. *14*, 1657–1664. https://doi.org/10.3892/ol.2017.6282.

Zhang, P., Wu, C., Liu, N., Niu, L., Yan, Z., Feng, Y., and Xu, R. (2014). Protocadherin 11 x regulates differentiation and proliferation of neural stem cell in vitro and in vivo. J. Mol. Neurosci. *54*, 199–210. https://doi.org/10.1007/s12031-014-0275-x.

Zong, Z., Pang, H., Yu, R., and Jiao, Y. (2017). PCDH8 inhibits glioma cell proliferation by negatively regulating the AKT/GSK3beta/beta-catenin signaling pathway. Oncol. Lett. *14*, 3357–3362. https://doi.org/10.3892/ol.2017.6629.

STAR★METHODS

KEY RESOURCES TABLE

REAGENT or RESOURCE	SOURCE	IDENTIFIER
Antibodies		
Mouse HA Tag monoclonal antibody (clone 2–2.2.14)	Thermo Fisher Scientific	Cat#26183; RRID: AB_10978021
Rabbit GFP polyclonal antibody	Thermo Fisher Scientific	Cat#A-11122; RRID: AB_221569
Sheep anti-digoxigenin-AP, Fab fragments polyclonal antibody	Roche	Cat#11093274910; RRID: AB_2734716
Sheep anti-digoxigenin-POD, fab fragments polyclonal antibody	Roche	Cat#11207733910; RRID:AB_514500
Sheep anti-fluorescein-POD, fab fragments polyclonal antibody	Roche	Cat#11426346910; RRID:AB_840257
Custom made anti-Pcdh19 polyclonal antibody	Biswas et al. (2010)	NA
Peroxidase-AffiniPure goat anti-mouse IgG (H + L) antibody	Jackson ImmunoResearch Labs	Cat#115-035-003; RRID:AB_10015289
Peroxidase-AffiniPure goat anti-rabbit IgG (H + L) antibody	Jackson ImmunoResearch Labs	Cat#111-035-003; RRID:AB_2313567
Alexa fluor 594 goat anti-mouse IgG (H + L)	Molecular Probes	Cat# A-11008; RRID:AB_143165
Alexa fluor 488 goat anti-rabbit IgG (H + L)	Molecular Probes	Cat#A-11005; RRID:AB_141372
Chemicals, peptides, and recombinant proteins		
RNA labeling mix with digoxygenin-11-dUTP	Roche	Cat# 11277073910
RNA labeling mix with fluorescein-12-dUTP	Roche	Cat# 11685619910
16% paraformaldehyde	Electron Microscopy Sciences	Cat# 15,710
XAV939	Cayman Chemicals	Cat#13596; CAS No. 284028-89-3
NBT/BCIP	Sigma-Aldrich	Cat#11681451001
cOmplete, mini, EDTA-free protease inhibitor cocktail	Sigma-Aldrich	Cat#11836170001
Pierce Anti-HA magnetic beads	Thermo Fisher Scientific	Cat# 88,836
Western Lightning plus ECL substrate	Perkin Elmer	Cat#NEL103001EA
Critical commercial assays		
Ambion T3 mMessage machine kit	Thermo Fisher Scientific	Cat#AM1348
Ambion T7 MAXIscript kit	Thermo Fisher Scientific	Cat#AM1314
Ambion SP6 mMessage machine kit	Thermo Fisher Scientific	Cat#AM1340
Riboprobe T7 *in vitro* transcription system	Promega	Cat#P1440
TSA plus Amplification kit	Perkin Elmer	Cat#NEL756001KT
SuperScript IV first-strand synthesis system	Thermo Fisher Scientific	Cat#18091050
Fugene HD	Promega	Cat#E2311
ddPCR supermix for probes (no dUTP)	Bio-Rad	Cat# 1863024
Experimental models: cell lines		
Human: HEK293 cells	ATCC	CRL-1573
Zebrafish: ZF4 cells	ATCC	CRL-2050
Experimental models: organisms/strains		
Zebrafish: pcdh19$^{os51/os51}$	Cooper et al. (2015)	ZFIN: ZDB-GENO-060207-1
Zebrafish: TgBAC(pcdh19-0.5hsp70:H2A-GFP)^{os75Tg}	This paper	ZDB-ALT-210716-7
Zebrafish: pcdh1a$^{os63/os63}$	This paper	ZDB-ALT-210712-3
Zebrafish: pcdh7a$^{os65/os65}$	This paper	ZDB-ALT-210712-4
Zebrafish: pcdh9$^{os67/os67}$	This paper	ZDB-ALT-210712-5
Zebrafish: pcdh17$^{os69/os69}$	This paper	ZDB-ALT-210712-6
Zebrafish: pcdh18b$^{os71/os71}$	This paper	ZDB-ALT-210712-7

(Continued on next page)

Continued

REAGENT or RESOURCE	SOURCE	IDENTIFIER
Zebrafish: $ryk^{os74/os74}$	This paper	ZDB-ALT-210712-8
Zebrafish: AB wildtype	ZIRC	ZDB-GENO-960809-7
Zebrafish: TL wildtype	ZIRC	ZDB-GENO-990623-2
Oligonucleotides		
Primers and probes, see Table S1, Eurofins Genomics	This paper	N/A
Recombinant DNA		
pISceI-5xUAS:dnTCF-HA	This paper	N/A
pISceI:5xUAS:Pcdh19-GFP	This paper	N/A
pCS2-hsp70:Gal4-VP16	This paper	N/A
BAC(pcdh18b:Gal4)	This paper	N/A
pDUAL-14xUAS:H2A-GFP/Lifeact-GFP	This paper	N/A
pISceI-5xUAS:Ryk-HA	This paper	N/A
pCMV:Ryk-HA	This paper	N/A
pCMV:Pcdh18b-GFP	This paper	N/A
pCMV:Pcdh1aΔCP-GFP	This paper	N/A
pCMV:Pcdh9ΔCP-GFP	This paper	N/A
pCMV:Pcdh17ΔCP-GFP	This paper	N/A
pCMV:Pcdh18bΔCP-GFP	This paper	N/A
pCMV:CD4-GFP	This paper	N/A
Software and algorithms		
FIJI	http://fiji.sc	RRID:SCR_002285
MatLab	MathWorks	RRID:SCR_001622
QuantaSoft Analysis Pro Software	BioRad Laboratories	RRID:SCR_008426
ggplot2	RStudio	RRID:SCR_014601
GraphPad Prism 6	http://www.graphpad.com/	RRID:SCR_002798
JMP Pro14	http://www.jmp.com	RRID:SCR_014242
ClustalW	https://www.genome.jp/tools-bin/clustalw	RRID:SCR_017277

RESOURCE AVAILABILITY

Lead contact

Further information and requests for resources and reagents should be directed to and will be fulfilled by the lead contact James Jontes (Jontes.1@osu.edu).

Materials availability

Individual zebrafish lines and plasmid constructs generated in this study will be provided upon request.

Data and code availability

- Upon request, all data reported in this paper will be shared by the lead contact, James Jontes (jontes.1@osu.edu).
- The original code for Matlab analysis is available upon request from the lead contact.
- Any additional information required to reanalyze the data reported in this paper is available from the lead contact upon request.

EXPERIMENTAL MODEL AND SUBJECT DETAILS

Zebrafish maintenance

Adult zebrafish (Danio rerio) and embryos of the Tübingen longfin (TL) and AB strains were maintained at ~28.5°C in E3 buffer (5 mM NaCl, 0.17 mM KCl, 0.33 mM CaCl$_2$, 0.33 mM MgSO$_4$, pH 7.2) and staged as described in <u>The Zebrafish Book</u> (Westerfield, 1995). Wildtype strains used as controls were AB-TL in-crosses, and all transgenic and mutant lines were made in AB-TL background. Experiments were conducted on embryos between 14 and 48 hpf, which is prior to the age at which sex is determined in zebrafish. All zebrafish experiments and procedures were performed in compliance with institutional ethical regulations for animal research at Ohio State University and were approved by the university's Institutional Animal Care and Use Committee.

METHOD DETAILS

TALEN/CRISPR production of germline lesions

We used the online tool TAL Effector Nucleotide Targeter 2.0 (https://tale-nt.cac.cornell.edu/node/add/talen) to search for a TALEN target site in exon 1 of zebrafish *pcdh18b*. We identified an appropriate target site downstream of the signal peptide, CTGAAACTTATGCTTCTGGCggccgtggcgcacaaTGTTTCGGGGAAGACTTTAA (uppercase indicates TAL left and right binding sites). The TALEN arrays (left: HD-NG-NH-NI-NI-NI-HD-NG-NG-NI-NG-NH-HD-NG-NG-HD-NG-NH-NH-HD and right: NG-NG-NI-NI-NI-NH-NG-HD-NG-NG-HD-HD-HD-HD-NH-NI-NI-NI-HD-NI) were assembled in RCIscript-GoldyTALEN (Bedell et al., 2012) using the TAL Effector Kit 1.0 (Cermak et al., 2011). The plasmid kit used for the generation of TALENs was a gift of Daniel Voytas and Adam Bogdanove (Addgene kit #1000000016). Plasmid encoding assembled TALENs was linearized with SacI, and used as template for mRNA synthesis with a T3 mMessage Machine kit (Ambion). To generate germline lesions in zebrafish *pcdh18b*, we injected 1 cell stage embryos with 50 pg mRNA encoding the left and right nucleases. Injected embryos were grown to adulthood and screened for germline lesions. For screening, adult F0 fish were outcrossed with wild types, and genomic DNA was prepared from eight embryos of each cross. High resolution melt analysis (HRMA) was used to identify putative founders (Dahlem et al., 2012). PCR products exhibiting aberrant melting curves were cloned and sequenced. F0 adults exhibiting frameshift mutations were outcrossed and the F1 embryos were grown to adulthood. To screen the adult F1 fish, genomic DNA was prepared from caudal fin clips screened by HRMA. These heterozygote F1 founders were outcrossed again and the F2 offspring were raised and screened to establish mutant lines. To obtain homozygous *pcdh18b*[os71] mutants, heterozygotes for each allele were in-crossed and embryos were grown to adulthood and genotyped by DNA sequencing. For experiments, homozygous mutant adult fish were in-crossed to generate homozygous mutant embryos.

Germline mutations for *pcdh1a*[os63], *pcdh7a*[os65], *pcdh9*[os67], *pcdh17*[os69] and *ryk*[os74] were generated using CRISPR/Cas9. Target sites were identified using either ZiFiT (partners.zifit.org/ZiFiT/) or with CRISPRscan (https://www.crisprscan.org). For each target site, top and bottom oligonucleotides were annealed to generate double stranded oligos with overhangs compatible with the BsaI sites of plasmid DR274 (Hwang et al., 2013). DR274 was a gift from Keith Joung (Addgene plasmid #42250; http://n2t.net/addgene:42250; RRID:Addgene_42,250). Plasmids encoding target site gRNAs were verified by Sanger sequencing. Each gRNA plasmid was linearized with DraI and used as template for RNA synthesis with a T7 MAXIscript kit (Ambion). Plasmid pCS2-nCas9n (Jao et al., 2013) encoding Cas9 was linearized with NotI and used as template for mRNA synthesis using an SP6 mMessage Machine kit (Ambion). pCS2-nCas9n was a gift from Wenbiao Chen (Addgene plasmid #47929; http://n2t.net/addgene:47929; RRID:Addgene_47,929). One-cell stage embryos were injected with 1 nL of 80ng/μL of Cas9 mRNA and 40 ng/μL gRNA. Injected embryos were grown to adulthood and screened for germline lesions, as described above. For the gRNA directed against *pcdh19*, we used the target site, GGGCTCAGATTAACCCATCG, which is within the sequence encoding EC1. For gRNA directed against *ryk*, we used the target site, CCTGCTGCTCGAAGGGGCC.

BAC recombineering and transgenesis

Transposon-mediated BAC transgenesis was used to generate *TgBAC(pcdh19-0.5hsp70:H2A-GFP)*[os75Tg/os75Tg], which expresses GFP-tagged Histone H2A under the direction of *pcdh19* regulatory elements. To elevate expression levels, we incorporated a ~500 bp *hsp70* basal promoter. This line exhibited an expression pattern identical to previously generated with from this BAC clone (CH211-156n5).

Phylogenetic analysis

ClustalW (https://www.genome.jp/tools-bin/clustalw) was used to generate the δ-pcdh phylogenetic tree, using the sequences for EC1-5.

Whole mount *in situ* hybridization

Riboprobes directed against either the δ-protocadherin extracellular or intracellular domain were synthesized by first amplifying approximately 1 Kb of the extracellular domain by PCR using 3 dpf cDNA, as described previously (Biswas et al., 2010, 2014; Blevins et al., 2011; Emond et al., 2009). A T7 RNA Polymerase binding site was included in each of the reverse primers, and these PCR products were used as templates for *in vitro* transcription (Promega). Antisense riboprobes were labeled with digoxygenin-dUTP or fluorescein-dUTP (Roche). Whole mount *in situ* hybridizations were carried out using standard methods (Westerfield, 1995). Briefly, embryos were fixed at 4°C overnight in 4% paraformaldehyde in PBS, dehydrated in a methanol series and stored in 100% methanol overnight at −20°C. They were rehydrated in decreasing concentrations of methanol and embryos 24 hpf and older were permeabilized using Proteinase K (10μg/ml, Roche). Embryos were refixed in 4% paraformaldehyde prior to hybridization. Labeled riboprobe was added to the hybridization buffer at a final concentration of 200 ng/mL and hybridization was carried out at 65°C overnight. Alkaline phosphatase-conjugated anti-digoxygenin Fab fragments (Roche) were used at 1:5000 dilution. NBT/BCIP (Roche) was used for the coloration reaction. Images were captured on a Leica MZ16F stereomicroscope (Leica Microsystems). For double fluorescent *in situ* hybridization, embryos were fixed and hybridized with riboprobes against δ-protocadherins (labeled with digoxygenin-dUTP) and *her4.1* (labeled with fluorescein-dUTP). The digoxygenin-labeled probe was detected using anti-digoxygenin Fab-POD (Roche), and developed using the tetramethylrhodamine substrate from the TSA Plus kit (PerkinElmer). Subsequently, the fluorescein probe was detected with an anti-fluorescein Fab-POD (Roche) and developed using the fluorescein substrate from the TSA Plus kit. Embryos were imaged using two-photon microscopy as described below. Maximum projection images of 50 optical sections from each channel were generated in FIJI using the Smooth Manifold Extraction plug-in (Shihavuddin et al., 2017).

Coimmunoprecipitation and western blotting

HEK293 cells (CRL-1573, American Type Culture Collection) were transiently transfected with plasmids encoding GFP- or HA-tagged zebrafish protocadherins and Ryk using calcium phosphate precipitation as described previously (Cooper et al., 2015). As a negative control, cells were transfected with membrane targeted CD4-GFP and Ryk-HA. After 24 h, cells were rinsed in PBS and lysed on ice in cell lysis buffer (CLB) (20 mM Tris, pH 7.5, 150 mM NaCl, 1 mM EDTA, 0.5% Triton X-100, 1 mM PMSF, and 1X cOmplete protease inhibitor cocktail (Roche) and microcentrifuged at 4°C for 10 min. Supernatants were incubated with anti-HA magnetic beads (Thermo Fisher Scientific) overnight at 4°C. The beads were washed five times in wash buffer (20 mM Tris, pH 7.5, 150 mM NaCl, 0.5% Triton X-100), resuspended in loading buffer, and heated to 70°C for 10 min. Samples were loaded onto 10% Bis-Tris NuPAGE gels (Thermo Fisher Scientific) and subjected to electrophoresis. Proteins were then transferred (Bio-Rad Laboratories) to PVDF (GE Life Science), blocked with 5% nonfat milk in TBST, and incubated overnight with primary antibody (Thermo Fisher Scientific rabbit anti-GFP, 1:1,000; Thermo Fisher Scientific mouse anti-HA, 1:5,000). HRP-conjugated secondary antibodies (Jackson ImmunoResearch Laboratories) were used at 1:5,000, and the chemiluminescent signal was amplified using Western Lightning Plus (PerkinElmer). Blots were imaged on a molecular imaging system (Omega 12iC; UltraLum, Inc.). For *in vivo* coIP of Ryk-HA, 1-cell stage embryos were co-injected with plasmids pCS2: *-1.5hsp70: Gal4-VP16* and *5xUAS: Ryk-HA*. Embryos were heat shocked for 1 h at 14 hpf, and embryo extracts were prepared at 18 hpf. Embryos were lysed in CLB, as described above, and supernatants were incubated with anti-HA magnetic beads (Thermo Fisher Scientific) overnight at 4°C. Western blots were performed as described above (1:5,000 used for mouse anti-HA and 1:1,000 for rabbit anti-Pcdh19 primary antibodies; anti-Pcdh19 antibody custom made by Covance ((Biswas et al., 2010)).

ZF4 cell culture and immunocytochemistry

The zebrafish fibroblast cell line ZF4 (CRL-2050, American Type Culture Collection) was cultured in DMEM: F12 media (GIBCO) with 10% fetal bovine serum and maintained at 28°C. ZF4 cells were seeded on glass coverslips and transfected with plasmids encoding Pcdh19-GFP and Ryk-HA using Fugene HD (Promega) according to the manufacturer's protocol. Cells were fixed 24hr later with 4% paraformaldehyde in PBS for 10 min, permeabilized with 0.25% Triton X-100/PBS for 5 min, and rinsed thoroughly. Cells were then

incubated overnight at 4°C in blocking solution (PBS, 2% normal goat serum, 3% BSA) and primary antibodies (mouse anti-HA, Invitrogen; rabbit anti-GFP, Thermo Fisher Scientific). Cells were then immunolabeled with Alexa-conjugated secondary antibodies (Molecular Probes) and DAPI (Thermo Fisher Scientific) was added to visualize cell nuclei. Coverslips were rinsed and mounted in Fluoromount G (Electron Microscopy Science). Images were captured on an Andor spinning disk confocal system fitted with a Nikon TiE inverted epifluorescence microscope equipped with a 100x/1.4NA Plan-Apochromat VC oil immersion objective, a Lumencor SOLA LED light source for epifluorescence illumination, and an Andor iXon Ultra 897 EMCCD camera.

axin2 and lef1 transcript quantification

Total RNA was extracted from 18-hpf embryos using TRI Reagent (Sigma-Aldrich) and cDNA was synthesized using SuperScript IV First-Strand Synthesis System (Thermo Fisher Scientific). Digital droplet PCR (ddPCR) was used to quantify *axin2* and *lef1* transcript levels in mutant and WT embryos and normalized to *gapdh* expression. In brief, 15,000–18,000 droplets were generated with QX200 droplet generator (Bio-Rad). Each droplet contained cDNA, primers and probes for *gapdh* and either *axin2* or *lef1*, and 2X ddPCR SuperMix (Bio-Rad) and droplet generating oil. cDNA partitioned within these droplets were PCR amplified and fluorescence from these droplets detected by the QX200 droplet reader (Bio-Rad). The relative abundance of *axin2* and *lef1* transcripts was calculated using Poisson statistical distribution of fluorescence absorption and normalized to *gapdh* transcript level using QuantaSoft software (Bio-Rad). Two technical replicates and at least three biological replicates were performed for each sample.

Immunocytochemistry and two-photon imaging

Zebrafish embryos were fixed for 1 h in 4% paraformaldehyde in PBS, then rinsed thoroughly in PBS before permeabilizing in acetone at −20°C for 7 min. Embryos were then rinsed in water and then PBS +0.1% Tween 20 (PBST). Embryos were then blocked in PBST, 2% Roche blocking reagent, 1% DMSO, and 10% fetal bovine serum. Primary antibodies were added to the samples for overnight incubation (rabbit anti-phospho-Histone H3 (1:200; Cell Signaling); mouse anti-HA (1:500; Invitrogen)). Alexa 488 and 594 secondary antibodies were used at 1:500 (Thermo Fisher Scientific). Two-photon imaging of embryos was performed at room temperature on a custom-built resonant-scanning microscope (Light and Jontes, 2019) controlled by ScanImage (Pologruto et al., 2003). Excitation was provided by a Chameleon-XR Ti:Sapphire laser (Coherent, Inc.) tuned to 800nm. We used a Nikon 25x/1.1NA water immersion objective. Embryos were oriented dorsal side up in low-melting point agarose (Sigma Aldrich) and immersed in PBS. Image stacks of 128 optical sections were taken at 1 μm intervals (1024 x 1024 pixels). To assess the role of Wnt/β-catenin signaling in cell proliferation, embryos were treated with the inhibitor XAV939 (Cayman Chemical). The inhibitor was added to the embryos at a final concentration of 15 μM in E3 buffer starting at 14 hpf prior to fixation at 18 hpf for phospho-Histone H3 immunolabeling. In order to block Wnt signaling by overexpression of dnTCF, embryos were injected at the 1-cell stage with 25 ng/μL pCS2:hsp:Gal4-VP16 and 25 ng/μL pIScel:5XUAS:HA-dnTCF or pIScel:5XUAS:Pcdh19-GFP plasmids. The expression of HA-dnTCF or Pcdh19-GFP was initiated by heat shocking the embryos at 37°C for 1 h at 14 hpf, and the embryos were allowed to recover before fixation at 18 hpf for phospho-Histone H3 immunocytochemistry. In the case of HA-dnTCF, the embryos were sorted for strong anti-HA fluorescence prior to mounting and imaging.

Image analysis and cell counting

Images stacks were initially adjusted for brightness and contrast in Fiji (Schindelin et al., 2012). Maximum intensity projections were made to determine the boundary of the neural tube and a manual mask was drawn to exclude non-neural nuclei from the analysis. For cross-correlation, a template nucleus was generated by cropping a 16 × 16 × 32 region around a well-labeled, well-isolated nucleus from one of the image stacks. Automated cell counting was performed in MATLAB (www.mathworks.com). Both the template and the image stacks were padded to 1024 × 1024 × 256 and a 3D cross-correlation was performed. An initial threshold for the correlation peaks was set manually to detect as many nuclei as possible and to eliminate any spurious peaks. Once set, this threshold was used for all analyzed image stacks. Data are reported as mean ± SEM.

Timelapse imaging and analysis of M phase

Wild type or pcdh18b−/− mutant embryos at the 1-cell stage were injected with a BAC clone (CH211-154p8) (Biswas et al., 2014) that was modified to drive expression of Gal4-VP16 *BAC(pcdh18b:Gal4)* along

with a dual UAS plasmid that drives co-expression of Histone H2A-GFP and Lifeact-GFP. The Lifeact-GFP labels F-actin and serves as a marker of the cell surface and cell dynamics and the H2a-GFP labels nuclei and condensed chromosomes; together they are excellent labels of dividing neuroepithelial cells. At 16-hpf, embryos were screened for expression, embedded in agarose and imaged by laser-scanning two-photon microscopy. Image stacks of the hindbrain (50 sections spaced at 1 μm) were collected at 2 min intervals for up to 10 h. Cells undergoing division were identified and the duration of M phase for each identified division was determined. During divisions, nuclei, as labeled by Histone H2A-GFP, undergo the following sequence: they exhibit a rapid movement toward the apical surface of the neural tube, round up, condense, align at the metaphase plate, then undergo anaphase. As it has previously been described that the rapid movement of the nucleus to the apical surface corresponds to G2 phase (Leung et al., 2011), we measured M phase as lasting from the onset of nucleus rounding through cytokinesis.

QUANTIFICATION AND STATISTICAL ANALYSIS

For pairwise comparisons, a two-tailed Student's t-test was used. For comparisons among groups, a one-way ANOVA with Tukey HSD was used. Statistics were calculated either with JMP Pro 14 (www.jmp.com) or with GraphPad Prism 6 (www.graphpad.com). All graphs and error bars represent the mean +/− standard error (SEM). The sample sizes for each experiment (n) and extent of significance is included in Figure Legends $*p < 0.05$, $**p < 0.01$, $***p < 0.001$.